Charge dynamics of muonium centers in Si revealed by photoinduced muon spin relaxation

R. Kadono*
Institute of Materials Structure Science, High Energy Accelerator Research Organization (KEK), Tsukuba, Ibaraki 305-0801, Japan

R. M. Macrae† and K. Nagamine‡
The Institute of Physical and Chemical Research (RIKEN), Wako, Saitama 351-0198, Japan

(Received 23 May 2003; published 29 December 2003)

Muonium dynamics in crystalline Si has been studied in both *p*-type and *n*-type samples using the muon spin-relaxation technique combined with photoexcitation. Controlling the excess carrier density in this way has revealed the dynamics of charge-exchange cycles and transfer processes involving $Mu_{BC}^{0/+}$ and $Mu_T^{-/0}$. In particular, photoexcitation has provided access to processes involving hole capture not attained by conventional experimental techniques. As a consequence, strong evidence was found for the delayed formation of electrically inactive muonium states in both types of Si, suggesting a process of diffusion-limited direct interaction of muonium with dopant impurities (i.e., muonium passivation).

DOI: 10.1103/PhysRevB.68.245204 PACS number(s): 71.55.Cn, 76.75.+i

I. INTRODUCTION

Hydrogen isotopes including muonium (Mu, an analog of atomic hydrogen in which the proton is substituted by a positive muon) are the simplest atomic defect centers conceivable in crystalline solids and have for that reason been attracting considerable and continued interest in solid-state physics. In particular, since the revelation in the 1980s that hydrogen, present often as an inadvertent impurity, interacts with deliberately introduced dopant atoms in semiconductors with drastic effects on their bulk electronic properties, the study of hydrogen isotopes and related complex defects has been a central topic in the field of semiconductor physics.[1–5]

The study of muonium centers in semiconductors is complementary to direct studies of conventional hydrogen isotopes in many respects. First, it is virtually the only source of information on the electronic structure of *isolated* hydrogen isotopes, whereas much information on hydrogen *complexes* has been generated by various spectroscopic techniques such as infrared absorption. Second, the μSR (muon spin relaxation) technique has a natural time window determined by the muon lifetime ($\tau_\mu \simeq 2.2\ \mu$s) and thus dynamical processes related to muonium centers correspond to the early stage behavior of hydrogen isotopes directly upon their implantation into the semiconductor matrices. Third, the exceedingly light mass of Mu ($\frac{1}{9}$th of the proton mass) leads to enhanced quantum-mechanical effects in the dynamical properties of Mu such as diffusion as compared to heavier hydrogen isotopes. Besides these points, it is further noteworthy that information regarding muonium centers has rapidly been accumulated on a wide variety of semiconductors whereas information on conventional hydrogen to date is strongly concentrated on Si.

It is presently established that there are two distinct muonium states in *c*-Si (as in other elemental and compound semiconductors with zinc-blende structure), one (known as Mu_{BC}) sitting at the Si-Si bond center and characterized by a highly anisotropic hyperfine structure, the other presumed by inference from its isotropic hyperfine structure to be at the T_d site (known as Mu_T).[4,5] The latter, whose nontransient nature on the μSR time scale has been puzzling in the light of the widespread theoretical recognition of Mu_{BC} as the ground state in the adiabatic potential,[6] has been recently identified as a state quantum mechanically stabilized owing to its light mass.[7] The coexistence of Mu_{BC} and Mu_T naturally leads to several issues such as the origin of the bistability, the energetics of these species including their charged states, and so on. The combination of ''annealing'' studies and resonance methodology has proven useful in addressing these issues in the past.[8,9] Positive muons are implanted into the specimen with a typical energy of a few MeV in which range the final state upon thermalization (which is reached within 10^{-11} s) is presumed to be governed by statistical factors rather than the detailed local electronic environment. Thus, the system starts off from a nonequilibrium state (particularly at low temperatures) in the time window of μSR. This situation allows us to obtain dynamical information on Mu simply by observing its alteration as a function of temperature. However, while this approach is the conventional one, one must deal with a certain complexity caused by the fact that various channels to the equilibrium state open simultaneously upon temperature rise. This complexity can be partly resolved by using photoexcitation to control the excess carrier density independently of the lattice temperature. Because of the relatively long lifetime of excess carriers in Si ($\simeq 10^1$–$10^2\ \mu$s), their population can be regarded as persistent during the μSR time window. Moreover, the combination of this technique with the use of heavily doped samples where the density of majority carriers is governed solely by the dopant concentration provides a control experiment to elucidate the role of minority carriers involved in the dynamical process under photoexcitation.

The first attempt by Zürich group to observe the effect of illumination on muonium center in Si yielded a negative result, presumably due to the limited light intensity.[3] The experiment was performed using a continuous muon beam combined with a continuous light source, with sample heating considerations setting a limit on the usable light intensity. This difficulty can be removed by the use of a pulsed light

 ©2003 The American Physical Society

source synchronized with a pulsed muon beam. Using such a method, and employing the spin-resonance technique, the Stuttgart group has successfully observed a change in the Mu^+ resonance amplitude upon illumination.[10] Unfortunately, the resonance technique, in common with other time-integral techniques, is of limited utility for the study of transient phenomena such as charge state transitions occurring during photoexcitation, and to this end a time-resolved μSR technique using a pulsed muon beam and light source has been developed.[11]

In this paper we report on the muonium dynamics in B-doped (p-type) and P-doped (n-type) c-Si revealed by time-resolved μSR under photoexcitation. Earlier stages of this study including work on intrinsic Si, n-type Si, and n-type Ge can be found in several preceding publications.[11–13] In the following we model the role of photoexcitation on the muonium dynamics and argue the advantage of the technique over the conventional annealing method. Then, a current model of Mu states in c-Si is briefly introduced to define some dynamical parameters which are used to interpret the present result. The results in p-type Si are relatively easy to understand and are therefore presented first in the following section, followed by the results in n-type samples.

II. METHODOLOGY

It is clear from annealing experiments that muonium centers form a deep donor level in the upper half of the energy band gap in Si.[8] When Mu^+ and Mu^0 are the possible charge states (corresponding to Mu_{BC}), the processes of electron release and capture associated with muonium center are described by the following two rate constants:

$$Mu^0 \rightarrow Mu^+ + e^-: r_{0+} = \rho_{0+} \exp(-E_{0+}/kT) \quad \text{(release)}, \tag{1}$$

$$Mu^+ + e^- \rightarrow Mu^0: r_{+0} = \sigma_{+0} v_e n_e \quad \text{(capture)}, \tag{2}$$

where ρ_{0+} is the attempt frequency, E_{0+} is the activation enthalpy, σ_{+0} is the cross section for electron capture, v_e is the Fermi velocity, and n_e is the electron density at the bottom of the conduction band. The point is that the release process is activated by phonons and only minimally affected by the carrier density in the conduction band, whereas the capture process is governed by the carrier density. Here, we deliberately avoid the use of terms such as ''ionization'' to label the process since that term also describes processes such as $Mu^0 + h^+ \rightarrow Mu^+$ (a process the rate of which is predominantly determined by the hole ''capture'' cross section). In the true equilibrium state the carrier density in n-type Si at low temperatures is approximately given by

$$n_e \sim \frac{1}{\sqrt{2}} (N_D N_C)^{1/2} \exp(-E_D/2kT), \tag{3}$$

where N_D is the number of donor atoms, N_C is the effective density of states in the conduction band, and E_D is the energy of donor level measured from the bottom of the conduction band. As shown by Eq. (3), the carrier density increases exponentially with increasing temperature until it enters the saturation range (e.g., 150–500 K for P-doped Si) determined by the density of donor atoms. This effect develops in parallel with the electron release process which has an activation energy $\sim E_{0+}$ for Mu, making it difficult to distinguish these two effects.

The role of photoexcitation in this situation is to increase the carrier density n_e to n_e^* which leads to the increase of the capture rate r_{+0} to r_{+0}^* without changing r_{0+}. In the actual situation the process is cyclic with an exchange rate

$$\nu = \frac{r_{0+} r_{+0}}{r_{0+} + r_{+0}}, \tag{4}$$

where one would expect two different cases. That is to say, when $r_{0+} \gg r_{+0}$, the exchange rate is limited by the capture process and consequently a significant effect is expected upon the increase of n_e to n_e^*. On the other hand, little or no effect of photoexcitation is anticipated for the case $r_{+0} \gg r_{0+}$.

In the case of intrasite charge conversion, the temperature dependence of ν is controlled by the activation process irrespective of photoexcitation. In particular, when the system is in the equilibrium state, one can define the Fermi level E_F, which is determined by the density of donors/acceptors and the temperature. The probability for muonium to be neutral is

$$p_0 = \left[1 + \frac{1}{g} \exp\left(\frac{E_{0+} - E_F}{kT} \right) \right]^{-1}, \tag{5}$$

where g is the ground-state degeneracy of the muonium impurity level (which is presumed to be 2 to accept one electron with either spin) and E_F is measured from the bottom of the conduction band. This would mean that muonium is neutral in n-type Si only over a low-temperature region determined by the condition $E_{0+} - E_F < 0$ and is always positively charged in p-type Si. However, as is shown later, the fact is that a large fraction of implanted muons are found to be neutral on an early time scale ($< 1\,\mu$s) even in moderately p-type samples, demonstrating that the implanted muons are in a nonequilibrium state at low temperatures. Nevertheless, the position of the Fermi level tells us whether or not charge conversion is favored in a given situation, and it thus remains a useful device for interpretation of the observed phenomena.

The presence of a cyclic charge-exchange process is detected through a longitudinal spin relaxation of muonium. Since the electrons are unpolarized, muon polarization is partly lost upon muonium formation: e.g., for Mu_T centers under a longitudinal field B,

$$P_T(B) = \frac{\frac{1}{2} + x^2}{1 + x^2}, \tag{6}$$

where $x = 2\Gamma_+ B/\omega_0$ with $2\Gamma_+ = \gamma_\mu + \gamma_e$, γ_μ and γ_e being the respective muon and electron gyromagnetic ratios, and ω_0 [$= 2\pi \times 2006.3$ MHz (Ref. 14)] is the muonium hyperfine frequency. In the strong collision model for a Markovian process where the muon spin loses its phase memory com-

pletely at each exchange step (whose approximation is valid for $\omega_0 \gg \nu$),[15] the time evolution of the muon polarization is described by

$$P_\alpha(t,B) \simeq \exp(-\nu t)\left\{ P_\alpha(B) + \nu \int_0^t [P_\alpha(B)]^2 dt_1 + \nu^2 \int_0^t \int_0^{t_2} [P_\alpha(B)]^3 dt_1 dt_2 + \cdots \right\}$$

$$= P_\alpha(B)\exp(-\nu t) \sum_{n=0}^{\infty} \frac{[P_\alpha(B)\nu t]^n}{n!}$$

$$= P_\alpha(B)\exp\{-\nu t[1-P_\alpha(B)]\}, \tag{7}$$

where $\alpha = \mathrm{T}$ or BC. For $\mathrm{Mu_T}$ centers the polarization expression becomes

$$P_\mathrm{T}(t,B) \simeq P_\mathrm{T}(x)\exp[-\lambda_\mathrm{T}(B)t], \tag{8}$$

$$\lambda_\mathrm{T}(B) \equiv \nu[1-P_\mathrm{T}(B)] = \frac{\nu}{2(1+x^2)}, \tag{9}$$

showing that the spin-relaxation rate is itself dependent on the applied field. While similar or identical results can be obtained by other approaches,[16–18] the above formulas are useful for an intuitive understanding of the origin of field-dependent relaxation. In particular, in the case of $\mathrm{Mu_{BC}}$ centers the muon polarization shows a complicated field dependence; that is, when $\gamma_e B \gg |\Gamma|, \Omega$ we have

$$P_\mathrm{BC}(B) = \frac{1}{8}\sum_{i=1}^{4}\left\{ \frac{(\Omega_i - \gamma_\mu B)^2}{\Gamma_i^2 + (\Omega_i - \gamma_\mu B)^2} + \frac{(\Omega_i + \gamma_\mu B)^2}{\Gamma_i^2 + (\Omega_i + \gamma_\mu B)^2} \right\}, \tag{10}$$

$$\Omega_i = \tfrac{1}{2}(\omega_\parallel \cos^2\theta_i + \omega_\perp \sin^2\theta_i),$$

$$\Gamma_i = \tfrac{1}{2}(\omega_\parallel - \omega_\perp)\sin\theta_i \cos\theta_i,$$

where $\omega_\parallel$ $(=2\pi \times 16.819$ MHz) and $\omega_\perp$ $(=2\pi \times 92.59$ MHz) are the anisotropic hyperfine parameters and θ_i is the angle between the field B and the $c[111]$ axis.[19,20] The function $P_\mathrm{BC}(B)$ has a broad minimum around a field

$$B_p \simeq \frac{\Omega_i}{\gamma_\mu}, \tag{11}$$

where the isotropic part of the effective hyperfine field on the muon is minimal and consequently the loss of muon polarization upon $\mathrm{Mu_{BC}}$ formation is at a maximum. This is also reflected in the spin relaxation of $\mathrm{Mu_{BC}}$ as

$$P_\mathrm{BC}(t,B) \simeq P_\mathrm{BC}(x)\exp[-\lambda_\mathrm{BC}(B)t], \tag{12}$$

$$\lambda_\mathrm{BC}(B) \equiv \nu[1-P_\mathrm{BC}(B)], \tag{13}$$

where $\lambda_\mathrm{BC}(B)$ shows a maximum at B_p. It should be stressed that these features allow us to distinguish readily between the two centers involved in the charge-exchange cycle without resorting to spin-rotation or resonance techniques.[21,22]

In addition to the cyclic charge/spin-exchange process, another important process which may occur is irreversible transition to another charge state, independently of the exchange process. In actual cases we often encounter a situation where muonium undergoing an exchange process and its associated spin relaxation slowly passes into a second stationary state with no spin relaxation. The time evolution of the muon polarization in this situation can be described by a two-state model. For example, when the initial state is one of these muonium states and transition to a nonrelaxing diamagnetic state occurs at a rate κ, we have

$$G_\alpha(t,B) = P_\alpha(t,B)e^{-\kappa t} + \kappa \int_0^t P_\alpha(u,B)q(t-u)e^{-\kappa u}du$$

$$= P_\alpha(B)\left[\frac{\lambda_\alpha}{\lambda_\alpha + \kappa} e^{-(\lambda_\alpha + \kappa)t} + \frac{\kappa}{\lambda_\alpha + \kappa} \right], \tag{14}$$

where $q(t)=1$ for the nonrelaxing final state. Two characteristic features may be pointed out for Eq. (14), namely (i) the net relaxation rate

$$\Lambda_\alpha(B) \equiv \lambda_\alpha(B) + \kappa \tag{15}$$

has a field-independent term κ and thus does not quench completely at higher field, and (ii) there is an asymptotic component

$$G_\alpha(\infty,B) = \frac{\kappa}{\lambda_\alpha(B) + \kappa} P_\alpha(B) \tag{16}$$

which also depends on the applied field. In the case of a $\mathrm{Mu_T}$ center converting to a diamagnetic state one obtains

$$G_\mathrm{T}(\infty,B) = \frac{\frac{1}{2} + x^2}{1 + \frac{\nu}{\kappa} + x^2}, \tag{17}$$

while $G_\mathrm{BC}(\infty,B)$ is more complicated. This feature is particularly useful when λ_α or κ is too large to resolve the initial relaxation [the first term in Eq. (14)] and only a residual component is observed in the μSR time spectra. For example, when the unseen paramagnetic state can be presumed to have an isotropic hyperfine structure, the hyperfine parameter ω_0 is readily determined by analyzing the field-dependent residual polarization with Eq. (17).

While examination of the magnetic-field dependence of the muon polarization provides a powerful technique to assist in the deduction of various dynamical and kinetic parameters, full investigation of the temperature dependence of all relevant parameters necessitates the collection of a very large quantity of data. Such a study is still beyond the scope of feasible experiment in terms of available beam time at existing muon facilities. Instead, we have chosen several points in temperature where characteristic and distinctive behavior is expected from earlier reports.

III. DYNAMICAL MODEL TO BE EXAMINED

Previous annealing studies in Si using the muon spin-resonance technique have led to the postulation of a dynami-

cal model involving transitions among four muonium states.[8,9] Results in *p*-type Si indicate that in this system transitions among Mu^0_{BC}, Mu^+_{BC}, and Mu^0_T states are sufficient for the interpretation of the data, whereas the Mu^-_T state becomes important in the *n*-type samples. The intrasite transitions ($Mu^0_{BC} \rightleftharpoons Mu^+_{BC}$ and $Mu^-_T \rightleftharpoons Mu^0_T$) are described by Eqs. (1) and (2). In addition, three further channels associated with site change between T and BC sites are introduced: these are the migration between neutral centers,

$$Mu^0_T \rightarrow Mu^0_{BC}, \tag{18}$$

and two channels associated with electron capture,

$$Mu^+_{BC} + e^- \rightarrow Mu^0_T, \tag{19}$$

$$Mu^0_{BC} + e^- \rightarrow Mu^-_T . \tag{20}$$

The presence of processes (18) and (19) is strongly suggested by the experimental evidence in intrinsic and *p*-type samples,[8,11,21] whereas process (20) is presumed to occur in *n*-type Si.[8]

However, the problem here is that relatively little is known about the shape of the adiabatic potential connecting these two sites. For example, pseudopotential density-functional theory studies of the system predict that there is no appreciable potential barrier between the T and BC sites.[6] The origin of the potential barrier (and hence that of the Mu bistability) might be related to dynamical behavior (e.g., the ''nonadiabatic'' response of the Si matrix to the muonium atom's motion), as we discuss later. For the time being we adopt a phenomenological potential[8,9] of the type illustrated in Fig. 1. Process (18) is then described by a simple activation expression similar to Eq. (1). The latter two processes are combinations of capture and activated site change, and so the rate, e.g., for process (19), might be governed by

$$t_{+0} = s_{+0} n_e v_e \exp(-H_{+0}/kT). \tag{21}$$

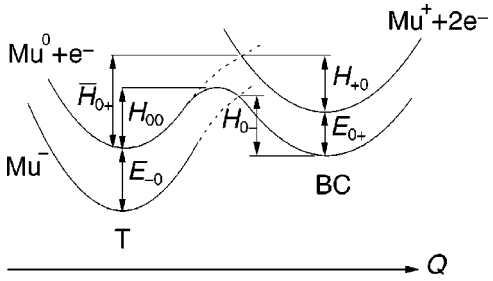

FIG. 1. Adiabatic potential model for muonium centers in Si (represented as a configuration coordinate). The energy for intrasite charge promotion is $E_{0+} = 0.21(1)$ eV for $Mu_{BC}(+/0)$ and $E_{-0} = 0.56(3)$ eV for $Mu_T(0/-)$. The activation enthalpies for the transitions involving site change are reported to be $H_{00} = 0.38(3)$ eV, $H_{+0} = 0.40(2)$ eV, and $H_{0-} = 0.31(1)$ eV (Ref. 9).

While the rate of this process is proportional to n_e and therefore susceptible to photoexcitation, it may be controlled by the factor $\exp(-H_{+0}/kT)$ at lower temperatures.

Because of the number of transitions potentially involved in the muonium dynamics it would be useful to sort them out according to their likely susceptibility to the photoexcitation. The relevant processes are listed in Table I for both *p*- and *n*-type samples. Among these, the following hole capture processes are added to the original model in Refs. 8 and 9;

$$Mu^0_T + h^+ \rightarrow Mu^+_{BC}, \tag{22}$$

$$Mu^-_T + h^+ \rightarrow Mu^0_T. \tag{23}$$

Note that the process, Eq. (22), has been already reported for intrinsic Si under photoexcitation.[11] Parameters for r_{+0}, r_{0+}, t_{+0}, $\bar{r}_{0+}$, t_{0-}, r_{0-}, r_{-0}, and t_{00} are reported in the literature,[8,9] where the first five have Mu_{BC} as the initial state, while the others have Mu_T. According to the literature values, the electronic state associated with $Mu_{BC}(+/0)$ lies about $E_{0+} = 0.21(1)$ eV below the conduction band. Recent

TABLE I. Transitions involved in the muonium dynamics in Si classified by release/capture of carriers, where those shown in boxes are processes added by the present work. The subscripts refer to the change of muonium state, and the overline refers to hole release/capture. The rates *r* are for intrasite processes while *t* are for intersite transfer processes. The processes in the left column are common to both *p*- and *n*-type Si whereas those in the right are presumed to occur only for *n*-type Si. The rates marked with an asterisk (*) can be increased by photoexcitation. Only the capture process is considered for holes, assuming that both $Mu_{BC}(+/0)$ and $Mu_T(0/-)$ levels lie in the upper half of the energy gap.

p- and *n*-type Si		*n*-type Si	
Electron vs Mu			
$r^{(*)}_{+0} = \sigma_{+0} v_e n_e$	$Mu^+_{BC} + e^- \rightarrow Mu^0_{BC}$	$r^{(*)}_{0-} = \sigma_{0-} v_e n_e$	$Mu^0_T + e^- \rightarrow Mu^-_T$
$r_{0+} = \rho_{0+} e^{-E_{0+}/kT}$	$Mu^0_{BC} \rightarrow Mu^+_{BC} + e^-$	$r_{-0} = \rho_{-0} e^{-E_{-0}/kT}$	$Mu^-_T \rightarrow Mu^0_T + e^-$
$t^{(*)}_{+0} = s_{+0} v_e n_e e^{-H_{+0}/kT}$	$Mu^+_{BC} + e^- \rightarrow Mu^0_T$	$t^{(*)}_{0-} = s_{0-} v_e n_e e^{-H_{0-}/kT}$	$Mu^0_{BC} + e^- \rightarrow Mu^-_T$
Hole vs Mu			
$\bar{r}^{(*)}_{0+} = \bar{\sigma}_{0+} v_h n_h$	$Mu^0_{BC} + h^+ \rightarrow Mu^+_{BC}$	$\bar{r}^{(*)}_{-0} = \bar{\sigma}_{-0} v_h n_h$	$\boxed{Mu^-_T + h^+ \rightarrow Mu^0_T}$
$\bar{t}^{(*)}_{0+} = \bar{s}_{0+} v_h n_h e^{-\bar{H}_{0+}/kT}$	$\boxed{Mu^0_T + h^+ \rightarrow Mu^+_{BC}}$		
Thermal			
$t_{00} = \rho_{00} e^{-H_{00}/kT}$	$Mu^0_T \rightarrow Mu^0_{BC}$		

study on *n*-type Si has revealed that the position of E_{-0} associated with $Mu_T(0/-)$ is 0.56(3) eV.[9] The activation enthalpies for the transitions involving site change seem to lie rather close together: for instance, $H_{00}=0.38(3)$ eV, $H_{+0}=0.40(2)$ eV, and $H_{0-}=0.31(1)$ eV, as illustrated in Fig. 1.[9] In any case, understanding of the potential-energy relationship between Mu^0_{BC} and Mu^0_T is currently based on the following pieces of evidence: (i) the transition from Mu^0_T to Mu^+_{BC} around 200 K fits a model of thermally activated transition from Mu^0_T to Mu^0_{BC} followed by electron promotion,[8] and (ii) the transition from Mu^0_T to Mu^0_{BC} is enhanced by photoexcitation near 10 K.[11]

In order to induce longitudinal spin relaxation of diamagnetic (charged) states, a cyclic succession of charge state transitions is required to take place. The following two processes, in which the charge state transition is controlled by electron capture/release at the BC site, are known to occur under thermal excitation.

*Cycle e*1. $Mu^0_{BC} \overset{r_{0+}}{\rightarrow} Mu^+_{BC}+e^- \overset{r_{+0}}{\rightarrow} Mu^0_{BC} \rightarrow \cdots$

$$\nu_{e1}=(r_{0+}^{-1}+r_{0+}^{-1})^{-1}=\frac{r_{0+}r_{+0}}{r_{0+}+r_{+0}}. \tag{24}$$

*Cycle e*2. $Mu^0_T \overset{t_{00}}{\rightarrow} Mu^0_{BC} \overset{r_{0+}}{\rightarrow} Mu^+_{BC}+e^- \overset{t_{+0}}{\rightarrow} Mu^0_T \rightarrow \cdots$

$$\nu_{e2}=(t_{00}^{-1}+r_{0+}^{-1}+t_{+0}^{-1})^{-1}=\frac{t_{00}r_{0+}t_{+0}}{r_{0+}t_{+0}+t_{00}t_{+0}+t_{00}r_{0+}}. \tag{25}$$

It is clear that these cycles are susceptible to the photoexcitation when the rate is controlled by the carrier capture process. In addition to these, we consider further cycles involving photo excited *holes* the presence of which is convincingly suggested by the present result on Mu_T centers in *n*-type Si.

*Cycle h*1. $Mu^-_T+h^+ \overset{\bar{r}_{-0}}{\rightarrow} Mu^0_T$, $Mu^0_T+e^- \overset{r_{0-}}{\rightarrow} Mu^-_T \rightarrow \cdots$.

$$\nu_{h1}=(\bar{r}_{-0}^{-1}+r_{0-}^{-1})^{-1}=\frac{\bar{r}_{-0}r_{0-}}{\bar{r}_{-0}+r_{0-}}. \tag{26}$$

*Cycle h*2. $Mu^-_T+h^+ \overset{\bar{r}_{-0}}{\rightarrow} Mu^0_T \overset{t_{00}}{\rightarrow} Mu^0_{BC}$,

$$Mu^0_{BC}+e^- \overset{t_{0-}}{\rightarrow} Mu^-_T \rightarrow \cdots$$

$$\nu_{h2}=(\bar{r}_{-0}^{-1}+t_{00}^{-1}+t_{0-}^{-1})^{-1}=\frac{\bar{r}_{-0}t_{00}t_{0-}}{t_{00}t_{0-}+\bar{r}_{-0}t_{0-}+t_{00}\bar{r}_{-0}}. \tag{27}$$

The primary goal of our work is to establish a self-consistent model of spin/charge dynamics including these cycles on the basis of energetics provided by Fig. 1. While the dynamical parameters reported in the literature are used to interpret the present data in "dark" (unilluminated) specimens, additional parts of the model extended to accommodate the effect of photoexcitation will be examined in the light of data obtained under illumination.

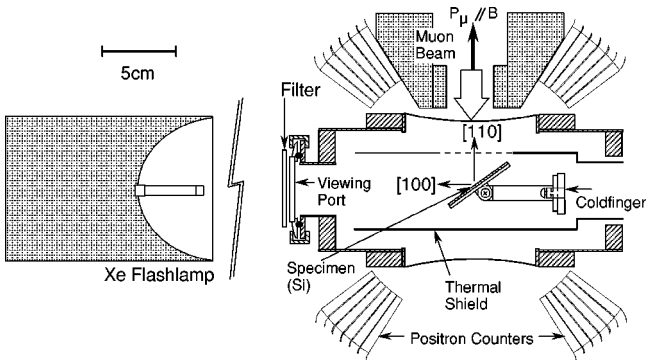

FIG. 2. A schematic diagram of the apparatus for the μSR measurement under photoexcitation. The Xe flash lamp provides a parallel light beam from the [100] direction.

It is inferred from the analysis based on the above dynamical model that there is a fraction of implanted muons which is unresponsive under illumination in both *p*- and *n*-type specimens, while no such component is observed in intrinsic Si. Our second goal is to demonstrate that this component is related to Mu-dopant atom interactions. The two-state model introduced in the preceding section will be used to describe the formation of such an inactive component.

IV. EXPERIMENT

The modern μSR experiment is based on the use of a so-called "surface muon" beam which is inherently 100% spin polarized along the beam direction and has a relatively low energy of 4 MeV. The implanted muons thermalize within $\sim$10 ps with a positional spread on the order of several tens of micrometers in Si, so that the density of self-created defects and vacancies in the immediate vicinity of each muon is negligibly small.[3] Thus, implanted muons may be regarded as simulating the situation pertaining in the extreme low-density limit of isolated hydrogen. This remains true even in the case of a pulsed muon beam where $\sim 10^3$–10^4 muons are delivered with every pulse.

The present experiment was conducted on the port 2 beam line at the RIKEN-RAL Muon Facility which provides a pulsed beam of surface muons ($\sim 10^4 \mu^+$ per pulse, 70 ns width, 50 Hz repetition). The thermal load upon photoexcitation was minimized by the combined effects of the extremely low duty factor of the pulsed light source (Xe flash lamp) and the pulsed nature of the muon beam. A schematic view of the setup around the specimen is shown in Fig. 2. A parallel light beam is delivered onto the Si wafer through a cutoff filter to eliminate photons of 700 nm or shorter wavelength which do not contribute to the bulk excitation. The excitation spectrum measured by μSR using band-pass filters indicates that photons in the energy range 1.2–1.4 eV (i.e., just higher than the energy gap for indirect electronic transitions in Si) dominate the bulk excitation. The photoinduced carrier density is then estimated from the photon intensity at the sample position measured by pyroelectric power meter and integrated over the appropriate energy range to yield

$$\sqrt{n_e^* n_h^*} \sim 1\times 10^{15}\ \text{cm}^{-3}. \tag{28}$$

TABLE II. Sample properties of the Si wafers including orientation, majority-carrier dopants, and their concentrations estimated from resistivity at ambient temperature.

Sample	Axis	Dopant	Type	C (cm^{-3})
p15	[100]	B	p	1.3×10^{15}–1.5×10^{16}
n15	[111]	P	n	6×10^{14}–1.5×10^{15}

This condition was common to all the runs carried out under photoexcitation. The characteristic properties of the Si specimens used in this study are listed in Table II. They were obtained from commercial sources as 4-in. wafers with mirror polishing on one side. The 4-in. wafers were Czochralski-grown crystals and so the concentration of oxygen impurities is likely to be relatively high compared with the float-zone Si used in most previous work. The apparatus was placed in the ARGUS spectrometer and time-differential μSR measurements were performed under a longitudinal field (LF-μSR). The longitudinal spin polarization $P_z(t)$ is proportional to the spatial anisotropy of decay positrons or ''asymmetry,''

$$A(t)=\frac{(1+\alpha)R_z(t)-(1-\alpha)}{(1+\alpha)-(1-\alpha)R_z(t)}=A_0P_z(t), \tag{29}$$

where A_0 is the asymmetry at the time origin (typically 0.2–0.3), $R_z(t)$ is the empirical ''raw'' asymmetry, which is deduced from the time histograms of the positron counters situated in positions either forward $(+)$ or backward $(-)$ with respect to the muon polarization,

$$N_{\pm}(t)=N_0^{\pm}\exp(-t/\tau_\mu)[1\pm A_0P_z(t)], \tag{30}$$

$$R_z(t)\equiv\frac{N_+(t)-N_-(t)}{N_+(t)+N_-(t)}, \tag{31}$$

TABLE III. The initial partition of muonium states in p15 and n15 samples determined by fitting to Eq. (34). The fraction f_P denotes a component which exhibits fast depolarization observed only in the n15 sample.

	p15			n15		
	37 K	150 K	280 K	12 K	150 K	290 K
f_T	0.40	0.47	0.53	0.40	0.35	0.65
f_{BC}	0.50	0.53	0.07	0.28	0.28	0.25
$f_{\pm}$	0.10	0.0	0.40	0.12	0.17	0.10
f_P				0.20	0.20	0.00

and $\alpha\equiv N_0^-/N_0^+$ is a correction factor originating in the difference in efficiency between the two sets of detectors. Note that for $\alpha=1$, $A(t)=R_z(t)$.

In the practical situation, there are two problems associated with the correction parameter α: (i) it occasionally drifts during long runs (i.e., over several hours) due to long-term instabilities in the muon beam delivery conditions, making it difficult to effect a precise comparison of the time spectra, and (ii) it often depends on the magnetic field, and consequently calibration data for $\alpha(B)$ are necessary in order to deduce the true underlying time spectra under longitudinal field. The former problem was resolved by adopting alternating mode data acquisition, where the flash lamp was fired only on every second beam pulse, and the time spectra with and without illumination were stored in separate sets of histograms. This feature proved helpful in minimizing systematic errors in comparing the two sets of μSR time spectra.

The origin of the field dependence in α is qualitatively accounted for through the angle dependence imposed on the positron energy spectra $\rho^{\pm}(E)$ by the different thicknesses of material through which the positrons must penetrate prior to their detection by the counters. The positrons undergo a spiral motion around the magnetic field with a radius propor-

TABLE IV. The dynamical parameters in p15 and n15 samples determined under the two-state transition model. The diamagnetic state denoted by $Mu'^{\pm}$ is the state which remains intact under photoexcitation probably due to the formation of Mu-dopant atom complex states. The rate r_{0+}^A is for the intrasite promotion of Mu_{BC} associated with acceptors, and r_{0-}^D for that of Mu_T or Mu_n associated with donors.

Sample	Transition/cycle	Parameter	Rate ($\times10^6$ s^{-1})		
p15			37 K	100 K	280 K
	ν_{e1}	ν	0.0	0.0	0.9
	$\nu_{e1}\simeq r_{0+}^A$	ν^*	1.3	2–10	0.85
	$Mu_{BC}^{+/0}\rightarrow Mu'^{+}$	κ'	0.33	0.0	0.13
n15			12 K	150 K	290 K
	r_{0-}^D (f_P)	ν_T	3.0	6.5	7.5
	$\nu_T+\nu_{h1}$ and ν_{h2}	ν_T^*	6.0	5.4	18
	$Mu_T^{0/-}\rightarrow Mu_T^-$	κ_T	~10	~13	2.5
	$Mu_{BC}^0/Mu_n^-\rightarrow Mu_T^-$	κ_{BC}	0.0	0.25	0.72
	r_{0-}^D (delayed)	ν_n	6.5	11	
	$\nu_n+\nu_{h1}$	ν_n^*	6.5	26	
	$Mu_T^{0/-}\rightarrow Mu'^{-}$	κ'	0.5	0.72	0.13

tional to the field intensity B. This motion prevents low-energy positrons from reaching the counters, so that the positron counts are given by

$$N_0^{\pm}(B) \propto \int_{E_{\min}(B)}^{E_{\max}} \rho^{\pm}(E)dE, \tag{32}$$

where $E_{\min}(B)$ is the threshold energy. This leads to $\alpha(B) = N_0^-(B)/N_0^+(B)$ which is thus field dependent in rather a complicated way. In the present work the calibration data for $\alpha(B)$ were obtained using an aluminum plate of similar shape and stopping density to the Si specimens. Because of a small degree of inaccuracy in reproducing the geometrical conditions in successive experiments, an offset value α_0 was necessary; each series of LF data was then fitted using the formula $\alpha'(B) \equiv \alpha(B) - \alpha_0$, where α_0, the zero-field value, was determined by matching it to $\alpha'_{\rm TF}$, the quantity extracted from a μSR spectrum obtained under a weak transverse field ($\simeq$20 G) and otherwise identical conditions,

$$\alpha'(0) \simeq \alpha'_{\rm TF} = \alpha(0) - \alpha_0. \tag{33}$$

We note that this calibration procedure for $\alpha(B)$ was quite satisfactory to obtain reasonable values for the asymmetry $A(t)$ under different external fields.

V. RESULTS AND DISCUSSION

As mentioned earlier, our measurements were mostly concerned with the detailed variation pattern of the muon polarization and its relaxation as functions of the magnetic field, with the aim of resolving the various muonium states through their field-dependent LF-μSR spectra. As a compromise, the variation in the temperature is rather limited; based on the results of resonance experiments,[8] we chose to take data at 37 K, 100 K, and 280 K in the p15 sample, and at 15 K, 50 K, 150 K, and 290 K in the n15 sample. These points represent three regions of temperature across which the charge/spin dynamics undergoes a major change as indicated by the difference of final-state population in both samples, namely, (1) below $\sim$50 K (''low-temperature region''), (2) 50–200 K (''intermediate temperature region''), and (3) above $\sim$200 K (''high-temperature region''). We will discuss the microscopic model of the charge/spin dynamics for each temperature region based on those representative data. The physical parameters determined in each temperature region are listed in Tables III and IV, where the values generally have relative uncertainty of about 10%.

A. The *p*-type samples

1. Low-temperature region (<50 K)

The LF-μSR time spectra in the p15 sample at 37 K are shown in Fig. 3 for the cases with and without photoexcitation (''light=on/off''). The field direction was parallel with the [110] axis (see Fig. 2). Upon photoexcitation, an asymptotic component [denoted by $A^*_{t=\infty} = A_0 P_z(\infty)$ in Fig. 3] is revealed to exist at this temperature, indicating the presence of a diamagnetic final state which does not interact with carriers. No such component was observed in intrinsic Si.[11]

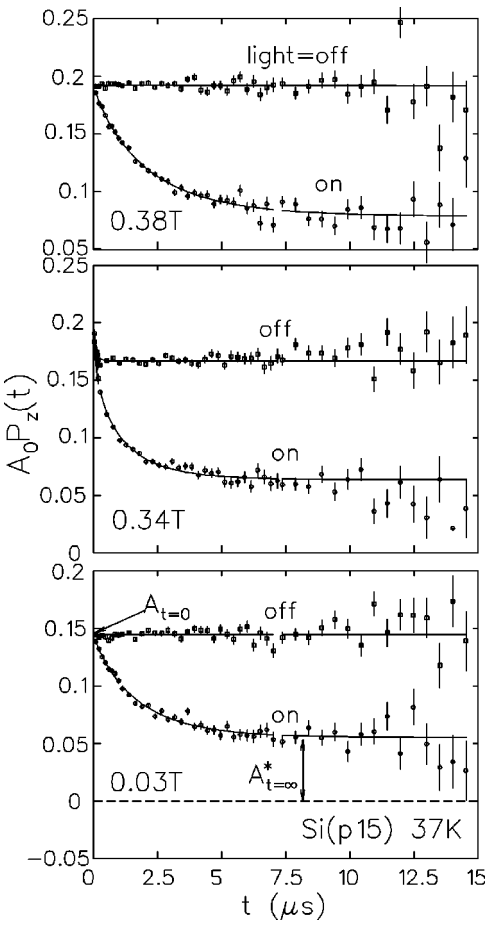

FIG. 3. μSR time spectra under a longitudinal field in p15 sample at 37 K, where an asymptotic signal is observed under photoexcitation (''light=on'').

Figure 4 summarizes the field dependence of the initial asymmetry [$A_{t=0} = A_0 P_z(0)$, common for light=on/off] $A^*_{t=\infty}$ and the spin-relaxation rate λ^* under photoexcitation. Assuming that the initial polarization is a sum over all possible muonium states, we have

$$A_{t=0} = A_0[f_{\rm T} P_{\rm T}(B) + f_{\rm BC} P_{\rm BC}(B) + f_{\pm}], \tag{34}$$

where $f_{\rm T}$, $f_{\rm BC}$, and $f_{\pm}$ are the fractional yields for $\mathrm{Mu}^0_{\rm T}$, $\mathrm{Mu}^0_{\rm BC}$, and $\mathrm{Mu}^{\pm}$, respectively. Fitting of the data in Fig. 4 to Eq. (34) yields values for f_α shown in Table III (with resulting $A_{t=0}$ shown by the solid curve), which is similar to that in intrinsic Si. (No significant change was reported below this temperature in earlier studies.) The small dips in $A_{t=0}$ are due to slight misalignment of the sample against the external field.

The component showing photoinduced spin relaxation (with a rate λ^*) exhibits features characteristic of a relaxation process involving $\mathrm{Mu}^0_{\rm BC}$; namely, the clear maxima predicted by Eq. (13) for $\lambda_{\rm BC}(B)$ are seen in Fig. 4(b). More specifically, the peak in the relaxation rate is given by Eq. (11) with an equally weighted combination of $(\cos^2\theta, \sin^2\theta) = (0,1)$ and $(2/3,1/3)$ for $B \| [110]$, yielding $B_p = 0.3415$ T and 0.1552 T corresponding to the two maxima in Fig. 4(b). This also indicates that the exchange rate is much slower

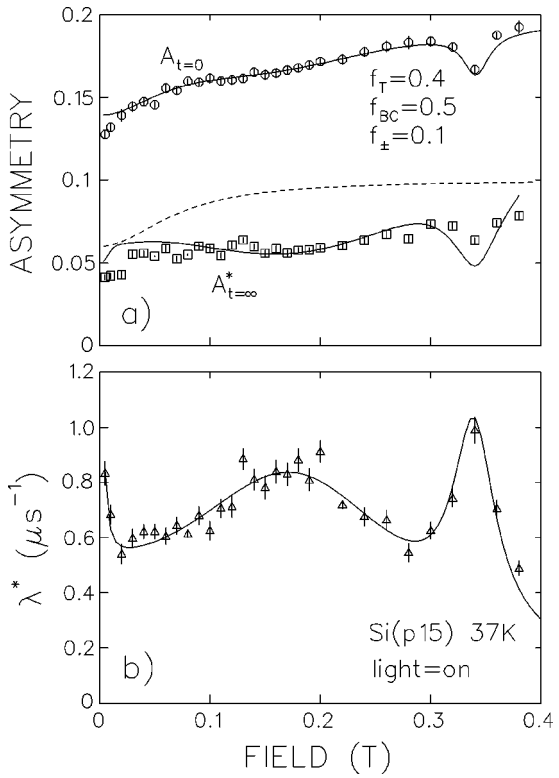

FIG. 4. Longitudinal field dependence of (a) the initial asymmetry ($A_{t=0}$) and asymptotic component ($A^*_{t=\infty}$), and (b) the spin-relaxation rate under photoexcitation, in p15 sample at 37 K. The solid curves in (a) are obtained by fitting to Eqs. (34) and (36), while the dashed curve is calculated for $A^*_{t=\infty}$ using Eq. (35) assuming that Mu^0_T remains unchanged under photoexcitation and that $\kappa'=0$. (The agreement becomes worse for $\kappa'>0$.) The solid curve in (b) is obtained using Eq. (13). All the solid curves were calculated assuming that the [110] axis makes an angle of 5° with the longitudinal field axis.

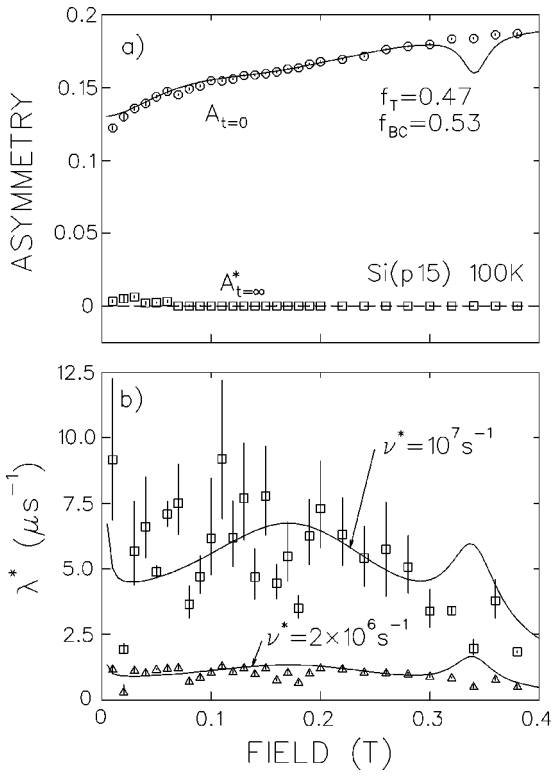

FIG. 5. Longitudinal field dependence of (a) the initial asymmetry ($A_{t=0}$) and asymptotic component ($A^*_{t=\infty}$), and (b) the spin-relaxation rate under photoexcitation, in the p15 sample at 100 K. The solid curve in (a) is obtained from fitting to Eq. (34), while those in (b) are obtained using $\lambda_{BC}(B)$ [Eq. (13)]. All the solid curves were calculated assuming that the [110] axis deviates from the LF direction by 5°.

than the hyperfine parameter of Mu^0_{BC}, which is consistent with the value obtained for the exchange rate, $\nu^*\simeq 1.3\times10^6\ s^{-1}$. (In the opposite limit, the peak structure is smeared out.) However, despite its large initial population ($\sim$40%), no trace of the Mu^0_T center is observed either in the spin relaxation or in the asymptotic component. We note that the field dependence of λ^* is entirely accounted for assuming a charge/spin-exchange process with Mu^0_{BC} as the intermediate paramagnetic state. Moreover, provided that the Mu^0_T state remains intact in the asymptotic component, we expect

$$A^*_{t=\infty}=A_0\left[f_T P_T(B)+f_{BC}P_{BC}(B)\frac{\kappa'}{\lambda^*+\kappa'}+f_\pm\right], \quad (35)$$

where κ' is the transition rate for Mu^0_{BC} to the final nonrelaxing state in the kinetic model described by Eq. (14). The notation marked with a prime refers to the parameter associated with the unknown final state, which we tentatively assign to a diamagnetic state labeled Mu'^+. The true character of Mu'^+ will be discussed later in view of the Mu-dopant atom interactions. As shown in Fig. 4 by the dashed curve, the observed field dependence of $A^*_{t=\infty}$ is quite different from the above prediction regardless of κ'. On the other hand, if the transition from Mu^0_T to Mu^0_{BC} is presumed to occur within a short time, one would expect

$$A^*_{t=\infty}=A_0\left[(f_T+f_{BC})P_{BC}(B)\frac{\kappa'}{\lambda^*+\kappa'}+f_\pm\right], \quad (36)$$

which is in good agreement with the data with $\kappa'\simeq 0.33\times10^6\ s^{-1}$. Since the rate of the thermally activated transition from Mu^0_T to Mu^0_{BC} described by t_{00} is negligible at 37 K, this observation leads us to conclude that a photoinduced transition from Mu^0_T to Mu^0_{BC} via the hole capture process, Eq. (22), occurs at this temperature. This is the same behavior as found in the case of intrinsic Si,[11] although the transition is not instantaneous in the p15 sample.

2. Intermediate temperature region (50–200 K)

The spin-relaxation rate under photoexcitation increases when the temperature is elevated from 37 K to 100 K. The asymptotic component observed at 37 K upon photoexcitation disappears at this temperature. The magnetic-field dependence of the asymmetry and relaxation rate are summarized in Fig. 5 with deduced values of f_α in Table III.

Although the origin of the two components in the relaxation rate is unknown at this stage, the field dependence is well described by $\lambda_{BC}(B)$ [Eq. (13)] in both cases with $\nu^* \simeq 2 \times 10^6$ s^{-1} and $\simeq 10^7$ s^{-1} for the respective components. It has in common with the result at 37 K that the initial Mu_T^0 state plays no role in the spin/charge-exchange process under photoexcitation. Considering that the initial muonium partition between Mu_T^0 and Mu_{BC}^0 is almost equal, it is plausible that one of the spin-relaxation rates is controlled by the rate for the hole capture process, $Mu_T^0 + h^+ \rightarrow Mu_{BC}^+$.

The increase of the photoinduced relaxation rate with temperature clearly indicates that, despite the strong effect of photoexcitation, the charge-exchange cycle is controlled by a thermally activated intrasite promotion process at the BC site with a rate r_{0+}^A. We find that $\nu^* \simeq r_{0+}^A \simeq 1.3 \times 10^6$ s^{-1} at 37 K which increases to $\simeq 10^7$ s^{-1} at 100 K. Assuming that

$$r_{0+}^A = \rho_{0+}^A e^{-E_{0+}^A/kT}, \tag{37}$$

one obtains $\rho_{0+}^A \simeq 3.4 \times 10^7$ s^{-1} and $E_{0+}^A \simeq 0.011$ eV from these two points, values far smaller than those obtained for the ionization process of Mu_{BC}^0. Although these values are quoted only as qualitative references, the further assumption of an additional rate component $\overline{r_{0+}^*}$ induced by photoexcitation, so that

$$r_{0+}^A = \overline{r_{0+}^*} + r_{0+}, \tag{38}$$

turns out to be incapable of accounting for the observed rate at 100 K as long as one assumes a constant value for $\overline{r_{0+}^*}$ and that $Mu_{BC}^0 \rightarrow Mu_{BC}^+ + e^-$ is the intrasite promotion process. These analyses lead us to speculate the presence of a thermal process involving boron acceptor centers,

$$Mu_{BC}^0 + B^0 \rightarrow Mu_{BC}^+ + B^-, \tag{39}$$

having a small activation energy. It is interesting to note that a similar process has been postulated in Ref. 8 with Mu_T^0 (instead of Mu_{BC}^0) as the initial state. This is in marked contrast with the case of the n15 sample, where no such process is observed over this temperature range.

3. High-temperature region (>200 K)

In contrast to the above low-temperature cases, the ionization rate of Mu_{BC}^0 by thermal activation is greatly enhanced at ambient temperature ($=3.4 \times 10^9$ s^{-1} at 280 K). As indicated by the result in intrinsic Si, the charge-exchange cycle is then controlled by the thermally activated process $Mu_T^0 \rightarrow Mu_{BC}^0$ [Eq. (18)] with a rate given by t_{00}. Note that the rate is quite sensitive to the temperature over this temperature range due to the large activation enthalpy ($H_{00} = 0.38$ eV).[9] The LF-μSR time spectra at 280 K exhibit a large asymptotic nonrelaxing component as those below 50 K. The magnetic-field dependence of the relevant parameters is summarized in Fig. 6.

As shown in Table III, a significant increase of $f_\pm$ (in place of f_{BC}) over lower temperatures is observed. This is readily attributed to Mu_{BC}^+ given the large ionization rate of

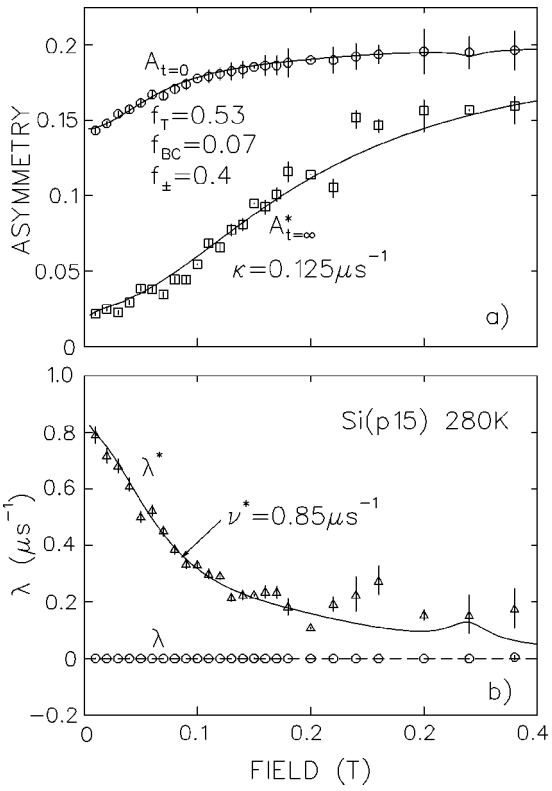

FIG. 6. Longitudinal field dependence of (a) the initial asymmetry ($A_{t=0}$) and asymptotic component ($A_{t=\infty}^*$), and (b) the spin-relaxation rate under photoexcitation, in p15 sample at 280 K. The solid curves in (a) are obtained by fitting to Eqs. (34) and (40), while that in (b) is obtained using a weighted average of $\lambda_T(B)$ and $\lambda_{BC}(B)$. All the solid curves were calculated assuming that the [110] axis deviates from the LF direction by 5°.

Mu_{BC}^0 at this temperature. The field dependence of λ^* is now much better described by a weighted average of $\lambda_T(B)$ and $\lambda_{BC}(B)$ [Eqs. (9) and (13)] with the exchange rate $\nu^* \simeq 0.85 \times 10^6$ s^{-1}. The strong field dependence is primarily characteristic of $\lambda_T(B)$, indicating that the primary intermediate paramagnetic state is Mu_T^0. This is in marked contrast with the case at lower temperatures. The exchange rate is in excellent agreement with the predicted t_{00}, supporting the scenario that Eq. (18) ($Mu_T^0 \rightarrow Mu_{BC}^0$) is the controlling process in the charge-exchange cycle.

Assuming that all of the Mu_T^0 and Mu_{BC}^+ present is involved in the charge-exchange cycle ("cycle *e*2" in Sec. III), the kinetic model to describe the transition to the second unknown stationary (nonrelaxing) state Mu'^+ predicts that

$$A_{t=\infty}^* = A_0 \left[(f_T + f_\pm) P_T(B) \frac{\kappa'}{\lambda^* + \kappa'} + f_{BC} P_{BC}(B) \right], \tag{40}$$

which is in good agreement with the data if $\kappa' \simeq 1.25 \times 10^5$ s^{-1}. The values of the relevant kinetic parameters are summarized in Table IV.

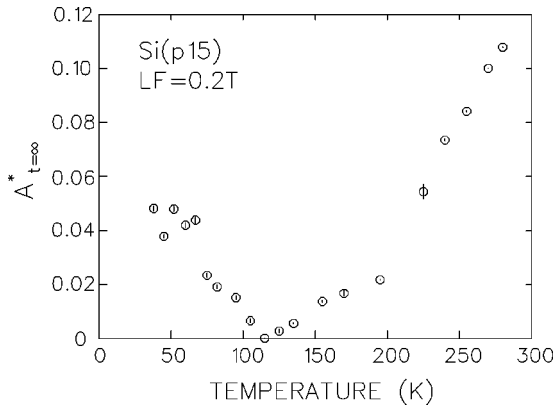

FIG. 7. Temperature dependence of the asymptotic component under photoexcitation, $A^*_{t=\infty}$, in p15 sample at 0.2 T. This quantity is proportional to $\kappa'/(\lambda^*+\kappa')$, where κ' is the transition rate to the final nonrelaxing state.

4. Asymptotic component under photoexcitation: Evidence for Mu passivation

The revelation of a nonrelaxing component $A^*_{t=\infty}$ under photoexcitation is one of the most important findings of our present result. The fact that this component is not involved in the charge-exchange cycle indicates that the state is not Mu^+_{BC} or Mu^0_{BC} in the ordinary sense. This point is further supported by the observation that the temperature dependence of $A^*_{t=\infty}$ shown in Fig. 7 is very different from that of the fractional yield for the delayed diamagnetic state obtained using muon resonance measurements in a sample corresponding to p15 (which shows a steplike increase above about 50 K and remains more or less constant between 100 K and 300 K).[8] As we show below, we found a similar component in our n15 sample, and this type of component is also found in *n*-type Ge.[13] Considering that this nonrelaxing component is observed only in these impurity-doped samples, the most probable situation is that the state is related to the dopant atoms. As mentioned earlier, we obtained $\kappa' \simeq 0.33 \times 10^6\ s^{-1}$ for the rate of transition to the final stationary state at 37 K. It should be noted that this rate is considerably smaller than r^A_{0+} ($\simeq 1.3\times 10^6\ s^{-1}$ at 37 K), and so this process cannot be the controlling process of the charge-exchange cycle. The same must be true at 280 K, where κ' is again much smaller than the exchange rate ν^* ($\simeq t_{00}$). Thus, we conclude that the process yielding $Mu^{'+}$is different from the intrasite promotion process at the BC site [Eq. (39)].

The fact that the asymptotic component is observed at 37 K and 280 K but not around 100 K, as seen from Fig. 7, suggests a microscopic model which involves a diffusion-limited process of interaction between Mu and the doped impurities, namely,

$$Mu^0_T + B^0 \rightarrow Mu^+_{BC} + B^-. \tag{41}$$

Note that the initial muonium state is different from that in Eq. (39). The irreversible character of the process suggests that the actual entity of $Mu^{'+}$is a Mu-*B* complex state, Mu^+_{BC} B^-. It is well established that the diffusion rate D_μ of Mu^0_T indeed exhibits such a temperature dependence in GaAs (Refs. 23 and 24) as well as in alkali halides.[25–27] The minimum of $D_\mu(T)$ occurs at the crossover temperature $T \simeq T_0$ between coherent quantum tunneling ($D_\mu \propto T^{-\beta}$, $T \ll T_0$) and phonon-assisted tunneling ($D_\mu \propto e^{-E_a/kT}$, $T \gg T_0$), where β is a positive constant (~ 3 in these crystals) and E_a is the thermal activation energy, which is on the order of 10^3 K. Consequently, the diffusion rate of Mu^0_T in GaAs at 30 K, for example, is comparable to that at 200 K where $D_\mu \simeq 5 \times 10^{-7}\ cm^2\ s^{-1}$. It is interesting to note that a similar situation has been suggested to pertain in Si, with a much higher diffusion rate.[3] According to an analysis of interaction between Mu^0_T and doped impurities based on a simple diffusion-limited trapping model, D_μ is greater than $10^{-4}\ cm^2\ s^{-1}$ around 20 K in Si. Provided that the direct Mu^0_T-acceptor interaction is described by the same kinetic model, one would expect the rate of direct interaction to be

$$\nu_A \simeq 4\pi D_\mu C_A r_A > 10^{12-13} \times r_A(\text{cm})\ \ s^{-1}, \tag{42}$$

where $C_A \simeq 10^{15-16}\ cm^{-3}$ is the acceptor concentration of the p15 sample and r_A is the effective range of the Mu^0_T-acceptor interaction. Thus, depending upon the magnitude of r_A, it may be that Mu^0_T tends to aggregate near the acceptor centers within a time scale shorter than that of photoinduced conversion from Mu^0_T to Mu^0_{BC}. Then, a possible scenario is that the Mu^0_{BC} centers formed later upon photoexcitation also tend to aggregate near the acceptor centers, with a subsequent slow kinetic process of Mu^0_{BC}-acceptor complex formation for which the rate is determined by κ'. While such a process may be unlikely for hydrogen at low temperatures due to the smaller influence of quantum effects on the diffusion kinetics, it is certainly likely to be the case for both muonium and hydrogen centers at higher temperatures ($>T_0$) where the diffusion rate is controlled by thermal activation.

B. The *n*-type samples

1. Low-temperature region (<50 K)

The behavior of muonium centers in *n*-type Si is markedly different from that in intrinsic and *p*-type Si in the sense that Mu^0_{BC} plays virtually no role as an intermediate paramagnetic state in the spin/charge dynamics. The absence of charge dynamics for Mu_{BC} at low temperatures (<150 K) is not surprising, considering that the rate for the promotion process, $Mu^0_{BC} \rightarrow Mu^+_{BC} + e^-$ (given by r_{0+}), is negligibly small due to the large activation energy ($E_{0+} \simeq 0.21$ eV). The position of the Fermi level is close to the bottom of the conduction band at low temperatures, which is also unfavorable for ionization. However, while about 25% of implanted muons form Mu^0_{BC} centers at higher temperatures, there is no sign of a cycle $e1$ process ($Mu^0_{BC} \leftrightarrow Mu^+_{BC} + e^-$) going on under photoexcitation. This is similar to the situation in intrinsic and *p*-type Si at ambient temperature, where cycle $e2$ ($Mu^0_T \rightarrow Mu^+_{BC} + e^- \rightarrow Mu^0_T \rightarrow \cdots$) dominates the process while the lifetime of the Mu^0_{BC} state is too short to involve it significantly. Moreover, the present data in *n*-type Si suggest that there must be a process other than Eq. (18) (Mu^0_{BC}

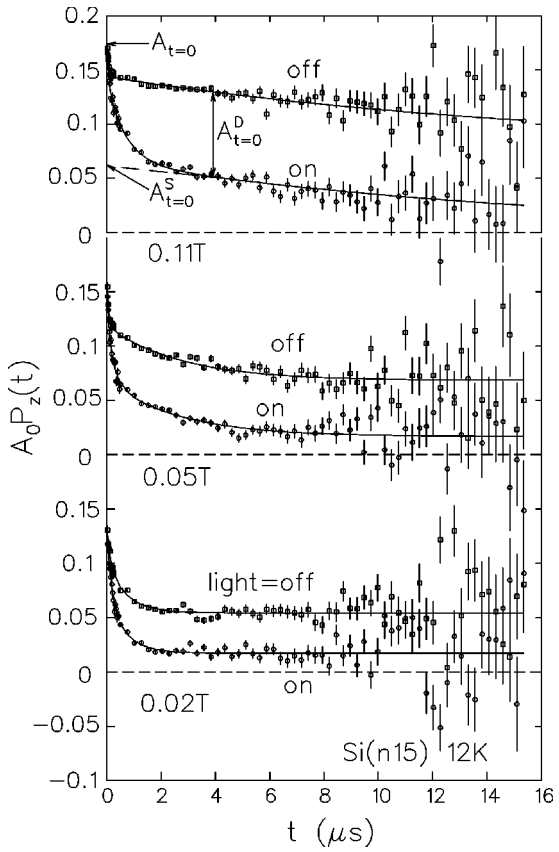

FIG. 8. μSR time spectra under a longitudinal field in the n15 sample at 12 K. There is a slowly relaxing component whose relaxation rate remains intact upon photoexcitation while the amplitude is reduced, indicating that there are two subcomponents, one susceptible to photoexcitation and one not, denoted by $A^D_{t=0}$ and $A^S_{t=0}$, respectively.

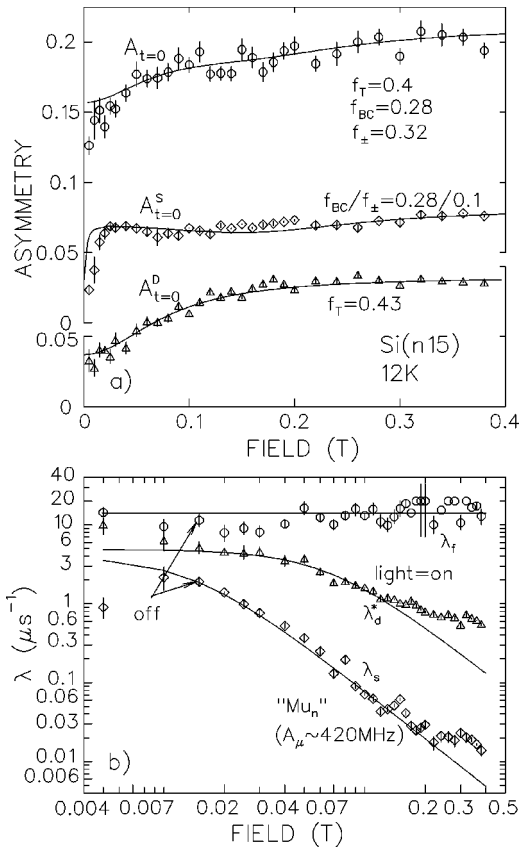

FIG. 9. Partial asymmetry (a) and spin-relaxation rate (b) vs applied longitudinal field in n15 sample at 12 K. The components are defined in Fig. 8. The solid curves are the results of curve fitting using the model described in the text.

$\rightarrow \mathrm{Mu}_\mathrm{T}^0$) to bridge between Mu_T and Mu_BC which underlies the fast spin/charge-exchange reaction at high temperatures.

Figure 8 shows some examples of the LF-μSR time spectra at 12 K. In contrast to p15 sample, one can clearly identify two components with different relaxation rates in the absence of photoexcitation ("light=off"). There is a rapidly depolarizing component ($\lambda_f \simeq 10^7\ \mathrm{s}^{-1}$) with a relative yield $f_P \simeq 0.2$. The spectra under photoexcitation indicate that the component with slow relaxation actually consists of two subcomponents, one susceptible to the photoexcitation and another with the relaxation rate unaffected. The magnetic-field dependences of the partial asymmetry components (defined in Fig. 8) and the corresponding relaxation rates are shown in Fig. 9. The total initial asymmetry $A_{t=0}$ is reproduced by Eq. (34) with the values of f_α in Table III (and the resulting $A_{t=0}$ is shown by the uppermost solid curve).

The component subject to the photoinduced spin relaxation exhibits the field dependence of a diamagnetic state (attributed to Mu_T^-) quickly converted from the precursor Mu_T^0 with fast spin relaxation, where the initial asymmetry for Mu_T^- is typically described by $G_\mathrm{T}(t,B)$ [Eqs. (14) and (17)], i.e.,

$$A^D_{t=0} = A_0 f_\mathrm{T} G_\mathrm{T}(\lambda_f t \gg 1, B)$$

$$= A_0 f_\mathrm{T} P_\mathrm{T}(B) \frac{\kappa_\mathrm{T}}{\lambda_f + \kappa_\mathrm{T}}$$

$$= A_0 f_\mathrm{T} \frac{\frac{1}{2} + x^2}{1 + \nu_\mathrm{T}/\kappa_\mathrm{T} + x^2}, \tag{43}$$

$$\lambda_f \simeq \frac{\nu_\mathrm{T}}{2(1+x^2)} + \kappa_\mathrm{T} \tag{44}$$

with ν_T and κ_T being the spin/charge-exchange rate of the precursor state and the conversion rate to the diamagnetic state, respectively. Note that there is no such process in the p15 sample. Fitting of the data to the above equation yields $\nu_\mathrm{T} \simeq 3 \times 10^6\ \mathrm{s}^{-1}$, $\nu_\mathrm{T}/\kappa_\mathrm{T} \simeq 0.25$, and $f_\mathrm{T} \simeq 0.43$, the last value slightly larger than that obtained from the analysis of the total initial asymmetry $A_{t=0}$. The difference implies that the fast relaxing component (f_P) is composed of the precursor Mu_T^0 (~ 0.03) together with another paramagnetic state ($\sim f_P - 0.03 = 0.17$) which appears nearly diamagnetic due to fast spin/charge exchange. As seen in Fig. 9, the relaxation rate of this component (λ_f) is almost independent of the magnetic field, indicating that the rate is primarily deter-

mined by a kinetic parameter. This is consistent with the above interpretation for the Mu_T^0 precursor, i.e., $\nu_T/2(1+x^2) \ll \kappa_T$ so that $\lambda_f \sim \kappa_T$. The situation would be the same for the rest of the fast relaxing component except that the exchange rate may be much higher than ν_T.

Since the thermal carrier concentration is nearly zero at 12 K, the extracted conversion rate κ_T ($\simeq 10^7$ s^{-1}) may be attributed to direct interaction between Mu_T^0 and dopant P atoms and/or the capture/release of transient carriers generated upon muon implantation. The same would be true for the process giving rise to ν_T at this temperature ($r_{0-} \simeq 0$ due to the large activation energy $E_{-0} \simeq 0.56$ eV). In any case, the final diamagnetic state is presumed to be Mu_T^- because it has the lowest formation energy in *n*-type Si. Thus, the rate κ_T describes the "thermalization" of implanted muons via a channel

$$Mu_T^0 + e^- \rightarrow Mu_T^- \quad \text{(epithermal)}, \tag{45}$$

and/or

$$Mu_T^0 + P \rightarrow Mu_T^- + P^+ \quad \text{(thermal)}. \tag{46}$$

The field dependence of the spin-relaxation rate under photoexcitation, λ_d^*, is qualitatively consistent with a spin/charge-exchange cycle with Mu_T^0 as the intermediate paramagnetic state. This supports the view that the charge-exchange cycle between Mu_T^0 and Mu_T^- is the dominant process under photoexcitation. More specifically, we found that

$$\lambda_d^* = \frac{\nu_T^*}{2(1+x^2)} + \kappa', \tag{47}$$

with $\nu_T^* \simeq 6.0 \times 10^6$ s^{-1} and the residual rate $\kappa' \sim 0.5 \times 10^6$ s^{-1}. The result of simplified curve fitting with κ' set to zero is shown in Fig. 9(b) by a solid curve. No clear asymptotic component associated with the transition κ' could be observed in the time spectra probably due to $\nu_T^*/\kappa' \gg 1$. Although the origin of the finite κ' is not clear at this stage, it suggests the presence of a slow kinetic process towards the equilibrium state.

It should be noted that the increase $\nu_T^* - \nu_T$ can be attributed to the cycle $h1$ via successive capture of photoexcited electrons and holes. Assuming that the cross section for hole capture at the T_d site is close to that for electron capture ($\bar{\sigma}_{-0} = \sigma_{0-} \simeq 1 \times 10^{-15}$ cm^{-2}), we have

$$\nu_T^* - \nu_T = \frac{\bar{r}_{-0}^* r_{0-}^*}{\bar{r}_{-0}^* + r_{0-}^*} \simeq \frac{\bar{r}_{-0}^*}{2} = \frac{1}{2}\bar{\sigma}_{-0} v_h^* n_h \sim 3 \times 10^6 \text{ s}^{-1}, \tag{48}$$

where $v_h^* = \sqrt{3k_B T^*/m_e}$ is the hole velocity related to the effective temperature T^* under photoexcitation. Since we have $n_h \simeq 1 \times 10^{15}$ cm^{-3} under photoexcitation, it leads to a crude estimation that $v_h^* \sim 6 \times 10^6$ cm/s or $T^* \sim 300$ K.

A corresponding analysis of the residual component under photoexcitation ($A_{t=0}^S$) indicates that it is composed of Mu_{BC}^0 and a part of the nonrelaxing diamagnetic state with the fractional yield $f_\pm \simeq 0.1$. However, the origin of the slow relaxation observed for Mu_{BC}^0 (irrespective of photoexcitation) seems not to be trivial. We have found that the field dependence of the relaxation rate λ_s is reproduced by none of the patterns expected for the known muonium states in Si. Surprisingly, it does not exhibit any enhancement around 0.2 T (or 0.35 T associated with some putative misalignment) characteristic of the spin/charge-exchange processes of Mu_{BC}^0 (see Fig. 4). On the contrary, it is rather well described by the behavior predicted for an *isotropic* muoniumlike entity having a small hyperfine parameter ω_n,

$$\lambda_s = \frac{\nu_n}{2(1+x_n^2)}, \tag{49}$$

where ν_n ($=\nu_n^*$) is the spin/charge-exchange rate and $x_n = 2\Gamma_+ B/\omega_n$. Curve fitting using the above relation yields $\nu_n \simeq 6.5 \times 10^6$ s^{-1} and $\omega_n \simeq 2\pi \times 420$ MHz, where the latter is far smaller than the known value of ω_0 for Mu_T^0 ($=2\pi \times 2006.3$ MHz). Tentatively, we suppose that this unidentified isotropic center "Mu_n^0" represents the effective dynamically averaged behavior of Mu_{BC}^0.

2. Intermediate temperature region (50–200 K)

The LF-μSR time spectra are qualitatively similar between 12 K and 150 K, allowing us to use the same procedure to analyze all spectra obtained over this range as was used for the 12-K data. One additional feature is that there is a shift of asymmetry from $A_{t=0}^D$ to $A_{t=0}^S$ at higher magnetic fields. We found that a kinetic model involving slow transition from Mu_{BC}^0 to Mu_T^- gives a satisfactory description of the data, i.e.,

$$A_{t=0}^D = A_0 \left[f_T \frac{\frac{1}{2} + x^2}{1 + \nu_T/\kappa_T + x^2} + f_{BC} P_{BC}(B) \frac{\kappa_{BC}}{\lambda_s^0 + \kappa_{BC}} \right], \tag{50}$$

and

$$A_{t=0}^S = A_0 \left[f_{BC} P_{BC}(B) \frac{\lambda_s^0}{\lambda_s^0 + \kappa_{BC}} + f_\pm \right], \tag{51}$$

$$\lambda_s = \lambda_s^0 + \kappa_{BC} = \frac{\nu_n}{2(1+x_n^2)} + \kappa_{BC}, \tag{52}$$

where κ_{BC} is the transition rate and λ_s^0 is the spin-relaxation rate of the initial Mu_{BC}^0 state which is presumed to follow Eq. (49). Note that the model used for the data at 12 K is obtained by setting κ_{BC} to zero. Curve fitting using the above equations leads to the results shown in Table IV; the fitted parameters indicate a slight increase in ν_T and ν_n as compared to 12 K.

Because of the complicated kinetic processes with different time scales involved in the spin dynamics, it is difficult to give a clear interpretation of the field dependence of the spin-

relaxation rate under photoexcitation. For simplicity we assume that the relaxation rate is the sum of all contributions at work, so that we have

$$\lambda_d^* \simeq \frac{\nu_{\mathrm{T}}^*}{2(1+x^2)} + \frac{\nu_{\mathrm{n}}^*}{2(1+x_{\mathrm{n}}^2)} + \kappa'. \tag{53}$$

As a matter of fact, we would fail to reproduce the data if we were to assume that the second term in the above form is absent. Curve fitting yields $\nu_{\mathrm{T}}^* \simeq 5.4\times10^6\ \mathrm{s}^{-1}$, $\nu_{\mathrm{n}}^* \simeq 2.6\times10^7\ \mathrm{s}^{-1}$, and $\kappa' \simeq 7.2\times10^5\ \mathrm{s}^{-1}$ (which includes a contribution from κ_{BC}). The value for κ' indicates that there is a gradual flow to the secondary diamagnetic state which is not affected by photoexcitation.

The effects of raising the temperature from 12 K to 150 K are summarized as follows. The fast relaxing component (f_P) is almost independent of temperature, indicating that the dynamical behavior of the precursor state is primarily determined by an epithermal relaxation (thermalization) process involving transient carriers. On the other hand, the fractional yield of nonrelaxing component ($f_\pm$) increases from 0.12 (12 K) to 0.17 (150 K) at the expense of $\mathrm{Mu}_{\mathrm{T}}^0$. Since an epithermal relaxation process would not depend on temperature, the increase in this component may be due to enhanced direct interaction of muonium with dopant atoms [e.g., Eq. (46)]. Moreover, a slow transition from $\mathrm{Mu}_{\mathrm{BC}}^0$ to $\mathrm{Mu}_{\mathrm{T}}^-$ (with a rate $\kappa_{\mathrm{BC}} \simeq 0.25\times10^6\ \mathrm{s}^{-1}$) is activated, with the result of increasing the diamagnetic component. The spin relaxation of $\mathrm{Mu}_{\mathrm{BC}}^0$, which seems to behave as if it were an isotropic Mu_{n} center, is enhanced as indicated by the increase of ν_{n} from 6.5 MHz (12 K) to 11 MHz (150 K). While the exchange process upon photoexcitation involving $\mathrm{Mu}_{\mathrm{T}}^0$ is unchanged (i.e., ν_{T}^* is about the same between 12 K and 150 K), a process involving the Mu_{n} center sets in to enhance the spin-relaxation rate under photoexcitation, as inferred from the large value of ν_{n}^*. Thus, the predominant channel of exchange is between Mu_{n} and $\mathrm{Mu}_{\mathrm{T}}^-$ at this temperature,

$$\mathrm{Mu}_{\mathrm{n}}^0 + \mathrm{P} \rightarrow \mathrm{Mu}_{\mathrm{T}}^- + \mathrm{P}^+. \tag{54}$$

Considering that the thermal activation of $\mathrm{Mu}_{\mathrm{T}}^-$ to $\mathrm{Mu}_{\mathrm{T}}^0 + e^-$ is negligibly small below 150 K, the observed increase in ν_{T}, ν_{n}, and ν_{n}^* strongly supports the presence of such an intrasite promotion process by a rate r_{0-}^D with small activation energy close to that for donors. The value of r_{0-}^D is on the same order of magnitude as these exchange rates at 150 K.

3. High-temperature region (>200 K)

Compared with those at 12 K and 150 K, the μSR time spectra at ambient temperature ($\simeq$290 K) are qualitatively different in the sense that the slow relaxation is quenched to leave a nonrelaxing asymptotic component ($\lambda_s = 0$). Moreover, the diamagnetic component with fast spin relaxation completely disappears at this temperature ($f_P = 0$); the fast relaxation is entirely from $\mathrm{Mu}_{\mathrm{T}}^0$ states (see below). This behavior is rather close to that in *p*-type Si at 37 K and at 280 K, suggesting that the situation is similar to or the same as that pertaining in these cases.

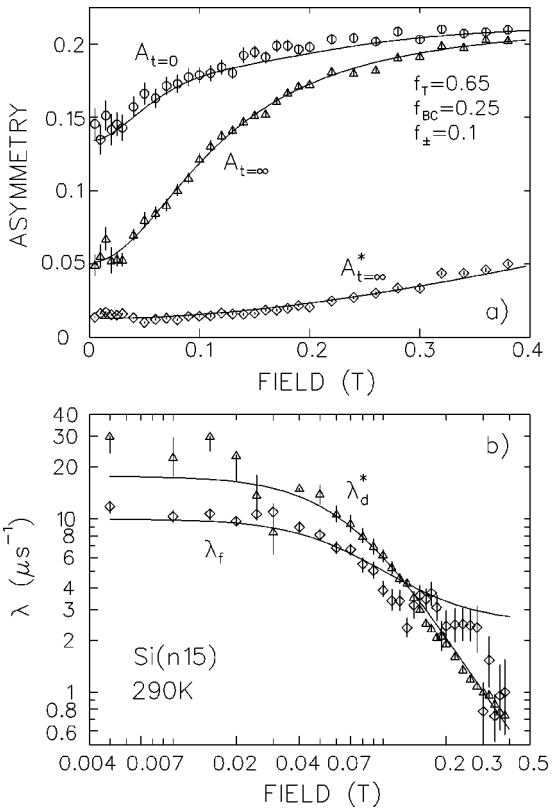

FIG. 10. Partial asymmetries (a) and spin-relaxation rates (b) vs applied longitudinal field in n15 sample at 290 K, where the definition of each component is given in the text. The solid curves are the result of curve fitting using the model described in the text.

Figure 10 summarizes the field dependences of the initial asymmetry [$A_{t=0} = A_0 P_z(0)$, common for light=on/off], the asymptotic asymmetries $A_{t=\infty}$, $A_{t=\infty}^*$, and the spin-relaxation rates with (λ^*) and without (λ) photoexcitation. The initial partition among the three muonium states is deduced to be $(f_{\mathrm{T}}, f_{\mathrm{BC}}, f_\pm) = (0.65, 0.25, 0.1)$ (yielding the resulting overall $A_{t=0}$ shown by the solid curve). Since f_{BC} is virtually unchanged throughout this temperature scan, the change in f_{T} must mainly be attributed to the recovery of initial $\mathrm{Mu}_{\mathrm{T}}^0$ fraction from the diamagnetic state showing fast spin relaxation at 150 K. Instead of a slow transition from $\mathrm{Mu}_{\mathrm{BC}}^0$ to $\mathrm{Mu}_{\mathrm{T}}^-$ at 150 K, we now find that a kinetic model with fast conversion of $\mathrm{Mu}_{\mathrm{BC}}^0$ to Mu_{T} gives the most satisfactory description of the data, i.e.,

$$A_{t=\infty} \simeq A_0 \left[(f_{\mathrm{T}} + f_{\mathrm{BC}}) \frac{\frac{1}{2} + x^2}{1 + \nu_{\mathrm{T}}/\kappa' + x^2} + f_\pm \right], \tag{55}$$

$$\lambda_f = \frac{\nu_{\mathrm{T}}}{2(1+x^2)} + \kappa_{\mathrm{T}} \tag{56}$$

and

$$A^*_{t=\infty}=A_0\left[(f_T+f_{BC})\frac{\frac{1}{2}+x^2}{1+\nu^*_T/\kappa'+x^2}+f_{\pm}\right], \quad (57)$$

$$\lambda^*_d=\frac{\nu^*_T}{2(1+x^2)}+\kappa'. \quad (58)$$

These terms are functionally similar to those presumed valid at 150 K, with $A_{t=\infty}$ corresponding to A^D+A^S and $A^*_{t=\infty}$ to A^S. The main difference is that there is no such state as Mu_n at this temperature; rather, all paramagnetic states behave as if they were Mu^0_T centers. Here, the suggested situation that the ratio $\kappa_{BC}/\lambda^0_s \gg 1$ in Eq. (50) is in line with the large transition rate t_{0-} for Eq. (20),

$$Mu^0_{BC}+e^- \rightarrow Mu^-_T,$$

where the parameter values in Ref. 9 yield $t_{0-}\simeq 10^8\ s^{-1}$ at 290 K. This in turn strongly suggests that the Mu_n center is a precursor of Mu^0_T. The results of curve fitting in Fig. 10 using the above equations are shown in Table IV.

In the case of the p15 sample, the Fermi level is always below the gap center and hence a channel for the promotion of Mu^0_{BC} to Mu^+_{BC} is available to the charge-exchange cycle at any temperature. The bottleneck in the Mu^+_{BC} channel (cycle $e2$), the predominant process at ambient temperature in the p15 sample, is the rate of the thermally activated transition from Mu^0_T to Mu^0_{BC} [Eq. (18), with a rate t_{00}]. On the other hand, in the n15 sample, the thermal activation of Mu^0_{BC} to Mu^+_{BC} is unavailable at lower temperatures due to the position of the Fermi level, leaving for Mu^-_T only via the cycle $h1$ involving hole capture.

The increase in ν^*_T at 290 K indicates that the exchange cycle is enhanced by a thermally activated process. One possibility is that cycle $e2$ (which is predominant in the p15 sample at ambient temperature) may dominate the exchange process. Unfortunately, the rate of the bottleneck reaction [Eq. (19)], t_{+0}, is estimated to be about $1.3\times 10^5\ s^{-1}$ at 290 K, which is too small to explain the value of ν^*_T at this temperature. Thus, alternative channel(s) of transition from the T_d to the BC site must be presumed to exist in order to explain the fast exchange interaction via the Mu^+_{BC} state in the n15 sample. Taking account of the present observation that Mu^0_T is the dominant paramagnetic state in the exchange cycle, we postulate a fourth process (which we term cycle $h2$),

$$Mu^-_T+h^+ \rightarrow Mu^0_T \rightarrow Mu^0_{BC}, \quad Mu^0_{BC}+e^- \rightarrow Mu^-_T \rightarrow \cdots.$$

We stress that the importance of holes in n-type Si has already been demonstrated in our earlier report on a strongly n-type sample.[12] Then, considering that $t_{0-} \gg \overline{r}_{-0}$, t_{00} in ν_{e2}, we have

$$\nu_T \simeq \frac{\overline{r}_{-0}t_{00}}{\overline{r}_{-0}+t_{00}}+r^D_{0-} \sim r^D_{0-} \simeq 7.5\times 10^6\ s^{-1} \quad (59)$$

in the dark specimen (where $\overline{r}_{-0}\simeq 0$), and

$$\nu^*_T \simeq \frac{\overline{r}^*_{-0}t_{00}}{\overline{r}^*_{-0}+t_{00}}+\nu^*_{h1}+r^D_{0-} \simeq t_{00}+\nu^*_{h1}+r^D_{0-} \simeq 1.8\times 10^7\ s^{-1} \quad (60)$$

under photoexcitation ($\overline{r}^*_{-0} \gg t_{00}$), where r^D_{0-} is the rate of other processes including incoherent electron/hole capture processes and direct Mu-donor interactions (see Table IV). Further assumption that

$$\nu^*_{h1} \simeq \nu^*_T(12\ K)-\nu_T(12\ K) \simeq 3.5\times 10^6\ s^{-1} \quad (61)$$

leads to a crude estimate of $t_{00}\sim 1\times 10^7\ s^{-1}$ at ambient temperature. This is in reasonable agreement with predictions based on the reported parameter values in the literature.[8,9]

4. Asymptotic component under photoexcitation: Evidence for Mu passivation

The field dependences of λ^*_d and $A^*_{t=\infty}$ at 290 K indicate that there is a slow process leading to the formation of a secondary diamagnetic state which is not susceptible to photoexcitation. It is interesting to note that the rate of this transition, κ', turns out to have almost the same value as the comparable transition in the p15 sample at 280 K. This agreement is a good piece of supporting evidence for an interpretation based on diffusion-controlled reaction of Mu^0_T centers with dopant atoms, given that both the diffusion rate of the Mu^0_T centers and the dopant atom concentration are common to the two cases. The earlier report of a larger asymptotic component ($\sim$90%) in more strongly n-type specimen ($[Sb]\sim 10^{18}\ cm^{-3}$) also supports such a scenario.[12]

The origin of the apparent difference in the amplitudes of the asymptotic components observed in p15 and n15 lies in the rate of spin/charge exchange under photoexcitation; $\nu^* \simeq 8.5\times 10^5\ s^{-1}$ in p15 whereas $\nu^*_T \simeq 1.8\times 10^7\ s^{-1}$. The increased value of ν^*_T at 290 K [compared to $\sim(5-6)\times 10^6\ s^{-1}$ below 150 K] indicates that the exchange cycle is controlled by a thermally activated process. Moreover, as shown in Fig. 11, the steplike increase in the amplitude susceptible to photoexcitation ($A_{t=\infty}-A^*_{t=\infty}$) indicates that, besides promotion of the diffusion process at temperatures above $\sim$200 K, there is an accompanying increase in some diamagnetic component. Assuming that there is an electronic energy level E_μ associated with the muonium state in the energy gap, Eq. (5) provides the probability that the muonium state in the n15 sample is electrically neutral,

$$p_0=\left[1+\frac{1}{g}\exp\left(\frac{E_\mu-E_F}{kT}\right)\right]^{-1}, \quad (62)$$

where E_μ is measured from the bottom of the conduction band. Curve fitting of the data in Fig. 11 using the above equation assuming $A_{t=\infty}-A^*_{t=\infty} \propto 1-p_0$ (with $g=2$) yields $E_\mu=0.21(1)$ eV. The value is surprisingly close to that for E_{0+} [$=0.21(1)$ eV], suggesting the possibility that the increase in the asymptotic component above 200 K is mainly due to the charge state promotion of Mu^0_{BC} to Mu^+_{BC}, whereas

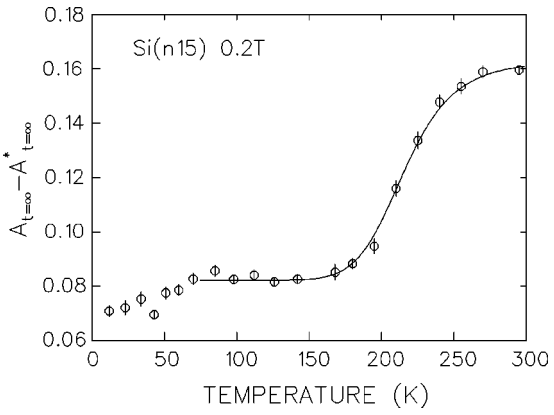

FIG. 11. Temperature dependence of the LF-μSR asymmetry susceptible to photoexcitation with LF=0.2 T (see text for the definition of $A_{t=\infty}$ and $A^*_{t=\infty}$). Solid curve is the result of fitting using a model described in the text.

it is controlled by the Mu-dopant interaction below 200 K. This is also consistent with the observation that the process involving Mu^0_{BC}, $Mu^0_{BC}+e^- \rightarrow Mu^-_T$, seems to set in above 200 K.

VI. SUMMARY AND CONCLUSIONS

It is known from annealing experiments using the muon spin-resonance technique (RF-μSR) that delayed formation of diamagnetic muon states ($Mu^{\pm}$) occurs in Si upon muon implantation.[8,9] Earlier work using RF-μSR combined with illumination has shown that photoexcitation has a strong effect on the spin dynamics of implanted muons in Si/Ge.[10] While continuous effort has been devoted to studies of this kind using the time-integrated techniques,[28,29] we have shown that time-differential μSR technique may in fact be a more useful approach for the detailed investigation of slow dynamics under photoexcitation.[11] In general one needs delayed-resonance techniques (where the RF pulse is irradiated some time after the initial spin relaxation) to distinguish between the initial spin relaxation and that in the final state only by RF-μSR. In the present work, we have shown using this time-differential μSR technique that there is a secondary diamagnetic state ($Mu'^{\pm}$) which remains intact under photoexcitation in both *p*-type and *n*-type Si. We have already reported a similar result for *n*-type Ge.[13] As typified by the p15 sample, the development of this electrically inactive state is well described by a two-state model with a transition rate $\kappa' \simeq 10^{5-6}$ s^{-1}. The kinetic parameters including other fast transitions referred in the text are summarized in Table IV.

The overall muonium dynamics in the p15 sample is well accounted for by consideration of a simple two-state model with slow conversion from a Mu^0_{BC} precursor (undergoing spin/charge-exchange reactions under photoexcitation) to $Mu'^{\pm}$. Besides this, detailed analysis indicates that there must be a fast transition from initial Mu^0_T to the precursor Mu^0_{BC} state upon photoexcitation via hole capture at low temperatures. Because of the absence of spin relaxation associated with this transition, it was not possible to deduce the value of the kinetic parameter (κ') associated with this process from the data using the two-state model. The local dynamics of the spin/charge-exchange interaction is similar to that in intrinsic Si, where either cycle $e1$ (at low temperatures) or cycle $e2$ (at ambient temperature) controls the process.

Compared with the situation in the p15 sample, the muonium dynamics in the n15 sample is far more complicated. There is a rapid dynamical process causing fast spin relaxation ($>10^7$ s^{-1}) which is marginally observable using present-day pulsed muon beam techniques. Detailed data analysis suggests that the process is controlled by rapid spin/charge-exchange interaction of a paramagnetic precursor state with transient carriers and/or dopant atoms. This fast exchange interaction, which is presumed to be quasiepithermal, is terminated by a kinetic process forming a diamagnetic state (Mu^-_T). The two-state model is demonstrated to be useful to describe the fast relaxation of Mu^0_T to Mu^-_T with rate parameter κ_T. After rapid thermalization, a slow transition from Mu^0_{BC} to a diamagnetic state (presumably Mu^-_T) is thermally activated with a rate κ_{BC} at 150 K. The photoinduced spin-relaxation behavior over this temperature range has revealed that $Mu^{0/-}_T$ must be serving as a recombination center (cycle $h1$), supporting the conjecture that the defect level associated with $Mu^{0/-}_T$ is located near midgap. Meanwhile, it became clear that Mu^0_{BC} exhibits a peculiar feature in its spin dynamics at low temperatures, behaving as if it were an isotropic Mu center with small hyperfine parameter (here called Mu_n). Although the state seems to correspond to an effective average of the dynamics between Mu^0_{BC} and Mu^0_T as seems a reasonable conclusion from its changes along with temperature, its true nature has yet to be clarified. Fortunately, this complication is removed at ambient temperature where the ambiguous Mu_n state disappears. All the Mu^0_{BC} centers are quickly converted to either Mu^-_T or Mu^+_{BC}, followed by intersite transition with the Mu^0_T state as the intermediate paramagnetic state in the local spin/charge dynamics (cycle $h2$). More interestingly, a small nonrelaxing asymptotic component appears at higher magnetic fields, in close parallel with the result in the p15 sample. Detailed analysis within the two-state model indicates that the rate of transition to the final nonrelaxing state (κ') is similar to that in the p15 sample at ambient temperature, supporting the scenario that the kinetic process is controlled by the diffusion-limited reaction of Mu with the dopant atoms.

The inactivity of the slowly formed diamagnetic state under photoexcitation is convincing evidence that the defect level associated with this state is not located within the energy gap. If it is true that these muons are located close to the dopant atoms, the whole process may be interpreted as a muonic analog of hydrogen passivation. The one reservation to wholehearted embrace of this hypothesis is that, despite years of effort, there has been no direct evidence of a muon-dopant atom complex state in Si. For example, if a muon-boron complex is formed in *p*-type Si, it should be readily observed by muon-nuclear level-crossing resonance.[30] To our knowledge, no such evidence has been reported to date with the single exception of a very weak signal purported to come

from a muon-Al complex in Al-doped Si.[31] However, this situation may be understood by considering a fast local tunneling process around four equivalent orientations of the complex state. Another possibility is that muonium is kept away from dopant atoms within the time scale of μSR ($\sim\mu$s) in the diffusion-limited reaction. According to an earlier study of interactions between Mu and impurity atoms in alkali halides,[32] the strain field around the impurity atom tends to intercept the tunneling diffusion of Mu towards the impurity atom at low temperatures due to the influence of the gradient in site energies as the impurity is approached. On the other hand, the activation energy for Mu tends to be smaller than that for H in their respective bound states due to the former's higher zero-point energy, and this may lead to a greater probability for Mu to be detrapped from impurities at higher temperatures. In any case, the electrostatic interaction can be long ranged (particularly at low temperatures where the screening carrier concentration is low), allowing charge-exchange interactions between muonium and dopant atoms to occur.

In conclusion, we have demonstrated the delayed formation of electrically inactive muonium states in both types of doped Si, suggesting a process of diffusion-limited direct interaction of muonium with doped impurities (i.e., muonium passivation). The use of the time-differential μSR technique combined with photoexcitation has shown itself to be a uniquely productive approach for the investigation of the electronic states of implanted muons in semiconductors, and in concert with more specific excitation using a laser source the method can be expected to mature into a powerful new tool for μSR spectroscopy of transient phenomena.

ACKNOWLEDGMENTS

We would like to thank the staff of RIKEN-RAL Muon Facility for the technical support during the experiment and RIKEN Accelerator Research Facility for providing computer resources for the data analysis. One of the authors (R.K.) acknowledges that the experimental part of this work was conducted while he was associated with RIKEN, and would like to acknowledge RIKEN for their general support. R.M.M. also wishes to acknowledge RIKEN for financial support.

*Also at School of Mathematical and Physical Science, The Graduate University for Advanced Studies.

†Present address: Natural and Behavioral Sciences Department, Marian College, Indianapolis, IN 46222-1997.

‡Present address: Institute of Materials Structure Science, High Energy Accelerator Research Organization (KEK), Tsukuba, Ibaraki 305-0801, Japan.

[1] *Hydrogen in Semiconductors*, edited by J. Pankove and N.M. Johnson (Academic, New York, 1990); S.J. Pearton, J.W. Corbett, and M. Stavola, *Hydrogen in Crystalline Semiconductors* (Springer, New York, 1992).

[2] S.M. Myers, M.I. Baskes, H.K. Birnbaum, J.W. Corbett, G.G. DeLeo, S.K. Estreicher, E.E. Haller, P. Jena, N.M. Johnson, R. Kirchheim, S.J. Pearton, and M.J. Stavola, Rev. Mod. Phys. **64**, 559 (1992).

[3] B.D. Patterson, Rev. Mod. Phys. **60**, 69 (1988).

[4] R.F. Kiefl and T.L. Estle, in *Hydrogen in Semiconductors*, edited by J. Pankove and N.M. Johnson (Academic, New York, 1990), p. 547.

[5] K.H. Chow, B. Hitti, and R.F. Kiefl, in μSR *on Muonium in Semiconductor and Its Relation to Hydrogen*, edited by M.J. Stavola, Semiconductors and Semimetals Vol. 51 (Academic, New York, 1998), p. 137.

[6] C.G. Van de Walle, P.J.H. Denteneer, Y. Bar-Yam, and S.T. Pantelides, Phys. Rev. B **39**, 10 791 (1989); Phys. Rev. Lett. **60**, 2761 (1988); K.J. Chang and D.J. Chadi, *ibid.* **60**, 1422 (1988); Phys. Rev. B **40**, 11 644 (1989).

[7] T. Miyake, T. Ogitsu, and S. Tsuneyuki, Phys. Rev. Lett. **81**, 1873 (1998).

[8] S.R. Kreitzman, B. Hitti, R.L. Lichti, T.L. Estle, and K.H. Chow, Phys. Rev. B **51**, 13 117 (1995).

[9] B. Hitti, S.R. Kreitzman, T.L. Estle, E.S. Bates, M.R. Dawdy, T.L. Head, and R.L. Lichti, Phys. Rev. B **59**, 4918 (1999).

[10] M. Iwanowski, K. Maier, J. Major, Th. Pfiz, R. Scheuermann, L. Schimmele, A. Seeger, and M. Hampele, Hyperfine Interact. **86**, 681 (1994).

[11] R. Kadono, A. Matsushita, R.M. Macrae, K. Nishiyama, and K. Nagamine, Phys. Rev. Lett. **73**, 2724 (1994).

[12] R. Kadono, R.M. Macrae, and K. Nagamine, Hyperfine Interact. **105**, 327 (1997).

[13] R. Kadono, R.M. Macrae, K. Nishiyama, and K. Nagamine, Phys. Rev. B **55**, 4035 (1997).

[14] E. Holzschuh, Phys. Rev. B **27**, 102 (1983).

[15] K.W. Kehr, G. Honig, and D. Richter, Z. Phys. B **32**, 49 (1978).

[16] I.G. Ivanter and V.P. Smilga, Zh. Éksp. Teor. Fiz. **60**, 1985 (1971) [Sov. Phys. JETP **33**, 1070 (1971)].

[17] W. Odermatt, Helv. Phys. Acta **61**, 1087 (1988).

[18] M. Senba, J. Phys. B **24**, 3531 (1991).

[19] Yu.M. Belousov, V.N. Gorelkin, and V.P. Smilga, Zh. Éksp. Teor. Fiz. **75**, 1999 (1978) [Sov. Phys. JETP **48**, 1007 (1978)].

[20] K.W. Blazey, T.L. Estle, E. Holzschuh, W. Odermatt, and B.D. Patterson, Phys. Rev. B **27**, 15 (1983).

[21] K.H. Chow, R.L. Lichti, R.F. Kiefl, S. Dunsiger, T.L. Estle, B. Hitti, R. Kadono, W.A. MacFarlane, J.W. Schneider, D. Schumann, and M. Shelley, Phys. Rev. B **50**, 8918 (1994).

[22] K.H. Chow, R.F. Kiefl, J.W. Schneider, B. Hitti, T.L. Estle, R.L. Lichti, C. Schwab, R.C. DuVarney, S.R. Kreitzman, W.A. MacFarlane, and M. Senba, Phys. Rev. B **47**, 16 004 (1993).

[23] R. Kadono, R.F. Kiefl, J.H. Brewer, G.M. Luke, T. Pfiz, T.M. Riseman, and B.J. Sternlieb, Hyperfine Interact. **64**, 635 (1990).

[24] R. Kadono, A. Matsushita, K. Nagamine, K. Nishiyama, K.H. Chow, R.F. Kiefl, W.A. MacFarlane, D. Schumann, S. Fujii, and S. Tanigawa, Phys. Rev. B **50**, 1999 (1994).

[25] R.F. Kiefl, R. Kadono, J.H. Brewer, G.M. Luke, H.K. Yen, M. Celio, and E.J. Ansaldo, Phys. Rev. Lett. **62**, 792 (1989).

[26] R. Kadono, R.F. Kiefl, E.J. Ansaldo, J.H. Brewer, M. Celio, S.R. Kreitzman, and G.M. Luke, Phys. Rev. Lett. **64**, 665 (1990).

[27] For a recent review, see, for example, V.G. Storchak and N.V. Prokof'ev, Rev. Mod. Phys. **70**, 929 (1998).

[28] R. Scheuermann, L. Schimmele, J. Schmidl, A. Seeger, Th. Stammler, E.E. Haller, D. Herlach, and J. Major, Hyperfine Interact. **105**, 357 (1997).
[29] R. Scheuermann, Appl. Magn. Reson. **13**, 195 (1997).
[30] Dj.M. Maric, P.F. Meier, S. Vogel, S.F.J. Cox, E.A. Davis, and J.W. Schneider, J. Phys.: Condens. Matter **3**, 9675 (1991).
[31] D.W. Cooke, M. Leon, M.A. Paciotti, B.L. Bennett, O.M. Rivera, S.F.J. Cox, C. Boekema, J. Lam, A. Morrobel-Sosa, P.F. Meier, T.L. Estle, B. Hitti, R.L. Lichti, E.A. Davis, J. Oostens, and E.E. Haller, Hyperfine Interact. **86**, 639 (1994).
[32] R. Kadono, R.F. Kiefl, W.A. MacFarlane, and S.R. Dunsiger, Phys. Rev. B **53**, 3177 (1996).